ELECTRO-OSMOTIC EFFECTS IN LOW REYNOLDS NUMBER FLOW THROUGH A PLANAR MICROFLUIDIC CONTRACTION-EXPANSION

Christian J. C. BISCOMBE, **Malcolm R. DAVIDSON, and Dalton J. E. HARVIE***

Department of Chemical and Biomolecular Engineering, The University of Melbourne, Parkville, Victoria 3010, AUSTRALIA

*Corresponding author, E-mail address: daltonh@unimelb.edu.au

ABSTRACT

Spurred by the growing interest in utilising electro-osmotic flow for microfluidic applications, a finite volume computational fluid dynamics (CFD) method is used to investigate steady electro-osmotic flows through a planar microfluidic contraction-expansion at low Reynolds number. The axial concentration profiles and pressure and potential changes occurring over the flow domain are compared with the results of two variants of a network theory that assumes that the flow within each distinct channel segment is fully developed. It is found that a model based on the matching of 'ion currents' (currents associated with the fluxes of individual ion species) exhibits better agreement with the CFD simulations than the alternative concentration-matching approach previously described in the electrokinetics literature.

Keywords: electro-osmosis, microfluidic, contraction, electrokinetic, numerical, ion current

NOMENCLATURE

A cross-sectional area, m^2
B dimensionless parameter
D diffusivity, $m^2\,s^{-1}$ or dimensionless
e elementary charge, C
$G_{i,\pm}$ dimensionless coefficients in Eqs. (13) and (14)
I electric current, A or dimensionless
K dimensionless inverse Debye length
k_B Boltzmann constant, $J\,K^{-1}$
L channel length, m
N_{kj} concentration ratio, dimensionless
$\hat{\mathbf{n}}$ dimensionless outward normal to channel wall
n ionic number concentration, m^{-3} or dimensionless
n_0 bulk ionic number concentration, m^{-3}
P pressure, Pa or dimensionless
ΔP pressure difference, Pa or dimensionless
Q volumetric flow rate, $m^3\,s^{-1}$
Re Reynolds number, dimensionless
S dimensionless surface charge density
Sc Schmidt number, dimensionless
T temperature, K
t time, s or dimensionless
U total electrical potential, V or dimensionless
ΔU potential difference, V or dimensionless
$\mathbf{v}$ liquid velocity, $m\,s^{-1}$ or dimensionless
V mean inlet velocity, $m\,s^{-1}$
W_{kj} half-width ratio, dimensionless
w half-width of inlet or outlet section of channel, m
x axial coordinate, m or dimensionless
δx dimensionless axial mesh spacing
y transverse coordinate, m or dimensionless
δy dimensionless transverse mesh spacing
z valency, dimensionless

Greek letters
ε liquid dielectric constant, dimensionless
ε_0 permittivity of free space, $C\,V^{-1}\,m^{-1}$
μ liquid viscosity, Pa s
ρ liquid density, $kg\,m^{-3}$
σ surface charge density, $C\,m^{-2}$
φ streaming potential, V or dimensionless
$\Delta\varphi$ potential difference, V

Superscript
(j) denotes condition within channel j

Subscripts
c   property of contracted section of channel
e   excess pressure or potential difference
i   property of inlet section of channel
o   property of outlet section of channel
t   total pressure or potential difference
+   property of cation
−   property of anion

Note that dimensionless variables are denoted either by a circumflex (CFD variables) or an overbar (network model variables) (see text).

INTRODUCTION

Over recent years, there has been a surge of interest in microfluidic technology, which promises to revolutionise chemical and biological analyses through the miniaturisation of complex processes onto small microchips. Such devices allow fluids to be manipulated with a very high degree of precision, which is essential for many separation, analysis, and manufacturing processes. The ever-broadening range of applications includes devices for protein crystallisation (Hansen *et al.*, 2002; Sauter *et al.*, 2007) and DNA analysis (Lagally *et al.*, 2000; Ugaz *et al.*, 2004).

Central to the efficient design and optimisation of microfluidic circuits is an understanding of the forces that govern transport phenomena in these systems. At the microscale, the influence of body forces is greatly diminished, while surface-based effects, such as surface tension and electrokinetic effects, become significant (Ho and Tai, 1998; Stone and Kim, 2001).

Electrokinetic phenomena arise when a charged solid

surface (e.g. channel wall) is brought into contact with an electrolyte (Hunter, 1981). The surface charges attract counter-ions in the liquid, and the interplay between electrostatics and diffusion leads to the formation of a thin charged region (the electrical double layer, or EDL) adjacent to the surface. The presence of the EDL gives rise to flow when an external electric field is applied across the channel. The field exerts a force on the charged fluid, which induces flow in the liquid bulk due to viscous drag. This phenomenon is known as electro-osmosis.

Liquid flow in microchannels can be driven either by an applied pressure gradient or electro-osmosis (or a combination of both). Electro-osmosis is particularly useful in narrow channels, where the pumping requirements for pressure-driven flow can become prohibitively large (Prakash *et al.*, 2008). Electro-osmosis has the advantages that the flow rate is proportional to the imposed potential gradient (Stone and Kim, 2001) and the velocity profile is uniform across the majority of the channel width (Park *et al.*, 2006). As such, electro-osmosis is frequently utilised for flow control in microfluidic devices (Bayraktar and Pidugu, 2006).

Electro-osmosis has been studied for channels of slowly varying cross-section (Ghosal, 2002; Park *et al.*, 2006), and also in more complex geometries including cross-flow and T-junctions (Dutta *et al.*, 2002a, 2002b). The aim of the present work is to investigate electro-osmotic effects in another non-uniform geometry: a two-dimensional planar 4:1:4 contraction-expansion.

COMPUTATIONAL FLUID DYNAMICS MODEL

We consider the steady flow of an incompressible, Newtonian binary electrolyte solution through a 4:1:4 planar contraction-expansion as shown in Fig. 1. Each section of the channel has the geometry of a thin Cartesian slit. The inlet and outlet sections have the same half-width, denoted by w. The lengths of the inlet, contraction, and outlet sections are taken to be equal, with $L_i = L_c = L_o = 10w$. The mean inflow velocity is V. We assume that the channel wall carries a net immobile charge of surface density σ. The dielectric constant of the wall material is taken to be much less than that of the liquid. We further assume that the liquid contains symmetric and equidiffusive cations and anions (denoted + and − respectively) with local (number) concentrations n_+ and n_- respectively. The bulk ionic concentration of the solution is n_0.

Governing Equations

Electrokinetic flows of ionic liquids are governed by a system of equations that includes momentum and continuity equations for the fluid, Nernst-Planck and conservation equations for each ion species, and a Poisson equation relating the total electrical potential to the local charge distribution. In dimensionless terms (where length, velocity, time, concentration, and electrical potential are scaled by w, V, w/V, n_0 and $k_B T/ze$ respectively), these equations are

$$\frac{\partial \hat{\mathbf{v}}}{\partial \hat{t}} + \hat{\nabla} \cdot (\hat{\mathbf{v}}\hat{\mathbf{v}}) = -\hat{\nabla}\hat{P} + \frac{1}{Re}\hat{\nabla} \cdot \left(\hat{\nabla}\hat{\mathbf{v}} + (\hat{\nabla}\hat{\mathbf{v}})^{\mathrm{T}} \right)$$
$$- \frac{BK^2}{Re}(\hat{n}_+ - \hat{n}_-)\hat{\nabla}\hat{U}, \qquad (1)$$
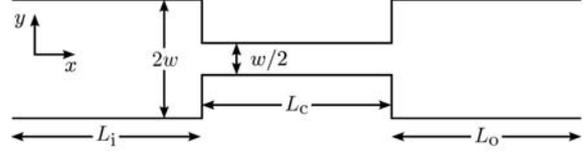
Figure 1: Schematic diagram of the 4:1:4 contraction-expansion flow geometry.

$$\hat{\nabla} \cdot \hat{\mathbf{v}} = 0 , \qquad (2)$$

$$\frac{\partial \hat{n}_+}{\partial \hat{t}} + \hat{\nabla} \cdot (\hat{\mathbf{v}}\hat{n}_+) = \frac{1}{ReSc}\left(\hat{\nabla}^2\hat{n}_+ + \hat{\nabla} \cdot (\hat{n}_+ \hat{\nabla}\hat{U}) \right), \qquad (3)$$

$$\frac{\partial \hat{n}_-}{\partial \hat{t}} + \hat{\nabla} \cdot (\hat{\mathbf{v}}\hat{n}_-) = \frac{1}{ReSc}\left(\hat{\nabla}^2\hat{n}_- - \hat{\nabla} \cdot (\hat{n}_- \hat{\nabla}\hat{U}) \right), \qquad (4)$$

$$\hat{\nabla}^2\hat{U} = -\frac{1}{2}K^2(\hat{n}_+ - \hat{n}_-) , \qquad (5)$$

where circumflexes denote dimensionless variables. The non-linear term on the left side of Eq. (1) is retained for completeness, although it is negligible for the low Reynolds number flows considered herein. The dimensionless numbers arising are

$$Re = \frac{\rho V w}{\mu}, \quad Sc = \frac{\mu}{\rho D},$$

$$B = \frac{\rho k_B^2 T \varepsilon_0 \varepsilon}{2z^2 e^2 \mu^2}, \quad K = \sqrt{\frac{2z^2 e^2 n_0 w^2}{\varepsilon_0 \varepsilon k_B T}}, \qquad (6)$$

where Re is the Reynolds number, Sc is the Schmidt number, B is a material property of the liquid (constant at fixed temperature), and K is the dimensionless inverse Debye length (*i.e.* the ratio of the channel width to the EDL thickness).

Boundary Conditions

The boundary conditions at the entrance of the channel are chosen to be consistent with fully developed electrokinetic flow. The inlet velocity and ion concentrations are based upon the analytical solution of Burgreen and Nakache (1964) for steady electrokinetic flow in a uniform two-dimensional Cartesian slit having the same width as the inlet. The axial potential gradient (electric field) at the inlet is chosen such that zero pressure gradient would be achieved in the equivalent uniform slit at steady state (*i.e.* the flow would be purely electro-osmotic).

The axial potential gradient at the outlet is assumed to be uniform and is chosen to satisfy Gauss's law applied over the flow domain (volume integral of Eq. (5) followed by application of the divergence theorem). The total current passing through the channel is non-zero in general. The lengths of the inlet and outlet segments are chosen such that flow at the entrance and exit of the domain is fully developed. Hence, axial gradients in velocity and the ion concentrations are taken to be zero at the outlet. The axial pressure gradient is chosen to ensure global mass conservation.

We set a potential boundary condition at the walls based on a uniform surface charge density. In dimensionless form, this boundary condition is

$$\frac{\partial \hat{U}}{\partial \hat{\mathbf{n}}} = S \equiv \frac{ze\sigma w}{\varepsilon_0 \varepsilon k_B T}, \qquad (7)$$

where $\hat{\mathbf{n}}$ denotes the outward unit normal at the channel wall, and S is the dimensionless surface charge density. In deriving Eq. (7), we have neglected the dielectric constant of the wall material, which is small compared to that of the liquid in many microfluidic systems. The other conditions at the wall are zero flux of ions normal to the wall and the no-slip velocity condition.

NETWORK MODELS

Several authors have described an analysis framework for microfluidic pipe networks based on fully developed flow in uniform channels (Ajdari, 2004; Berli, 2007; Xuan and Li, 2004). This framework consists of volume and charge conservation laws that must be satisfied around each node (or pipe junction) within the circuit:

$$\sum_{j=1}^{J} Q^{(j)} = 0, \qquad (8)$$

$$\sum_{j=1}^{J} I^{(j)} = 0. \qquad (9)$$

For a particular node, $Q^{(j)}$ and $I^{(j)}$ are the volumetric fluid flow rate and electric current respectively moving along channel j towards the node, and J is the number of channels that intersect at the node. The conservation laws apply to incompressible fluids in the absence of chemical reactions. A third equation is required to solve for the flow conditions within each channel. Several previous studies (Ajdari, 2004; Berli, 2007; Xuan and Li, 2004) have implicitly assumed that the bulk ionic concentration is constant throughout the network:

$$n_0^{(j)} = n_0^{(k)} \qquad (10)$$

for any two channels j and k. Harvie and Davidson (2009) have instead proposed that since electrical charge is carried by multiple ionic species in microfluidic systems, Eq. (10) should be replaced by a constraint on the current due to the motion of each individual ion species within the circuit. Defining $I_m^{(j)}$ as the current flowing along channel j in the direction of a specified node and due solely to the movement of ion species m, one may write

$$\sum_{j=1}^{J} I_m^{(j)} = 0 \qquad (11)$$

for each species $m = 1, 2, \ldots, M$ present within the fluid. Note that

$$I^{(j)} = \sum_{m=1}^{M} I_m^{(j)}, \qquad (12)$$

so that Eqs. (9) and (11) are consistent with each other.

Using Eqs. (8), (9), and (11), the pressure and potential differences along a microfluidic channel conveying a binary electrolyte solution can be related to the flow rate and ion currents within it (Harvie and Davidson, 2009):

$$1 = -\frac{1}{3}\overline{P} + G_1\overline{\varphi}, \qquad (13)$$

$$\overline{I}_\pm = \frac{1}{2}G_{2,\pm}\overline{P} - \left(G_{3,\pm} + \overline{D}_\pm G_{4,\pm}\right)\overline{\varphi}, \qquad (14)$$

where

$$\overline{P} = \frac{w^2 A}{\mu Q}\frac{\Delta P}{L}, \quad \overline{\varphi} = \frac{ezn_0 w^2 A}{\mu Q}\frac{\Delta \varphi}{L},$$

$$\overline{I}_\pm = \frac{I_\pm}{ezn_0 Q}, \quad \overline{D}_\pm = \frac{\mu D_\pm}{k_B T n_0 w^2} \qquad (15)$$

are the dimensionless pressure and potential changes over the length of the channel, the dimensionless ion currents, and the dimensionless diffusivities respectively. Eqs. (13) and (14) depend upon seven dimensionless G coefficients. Methods for evaluating these coefficients are presented by Harvie and Davidson (2009).

For a given set of inlet conditions, the preceding equations can be used to calculate idealised pressure and potential profiles for flow in a pipe network (such as a contraction-expansion). For a simple circuit in which several pipe segments are connected in series, each node represents the junction between coaxial segments, and Eqs. (6), (7), and (15) can be employed to derive the following relationships for any two segments j and k:

$$K^{(k)} = W_{kj}\sqrt{N_{kj}}K^{(j)}, \quad S^{(k)} = W_{kj}S^{(j)},$$

$$\overline{I}_\pm^{(k)} = \frac{\overline{I}_\pm^{(j)}}{N_{kj}}, \quad \overline{D}_\pm^{(k)} = \frac{\overline{D}_\pm^{(j)}}{W_{kj}N_{kj}^2}, \qquad (16)$$

where

$$W_{kj} = \frac{w^{(k)}}{w^{(j)}}, \quad N_{kj} = \frac{n_0^{(k)}}{n_0^{(j)}}. \qquad (17)$$

It also follows from Eqs. (12) and (16) that

$$\overline{I}^{(k)} = \frac{\overline{I}^{(j)}}{N_{kj}}. \qquad (18)$$

To solve for the pressure and potential conditions in pipe k under the matched current constraints of Eq. (11), an iterative procedure is adopted to determine a value of N_{kj} that satisfies Eqs. (8), (9), (11), (13), (14), (16), and (18). Alternatively, the (simpler) matched concentration condition of previous workers can be applied by noting that Eqs. (16) and (18) are consistent with Eq. (10) when $N_{kj} = 1$. In this circumstance, Eq. (11) will not be satisfied in general, so that it is not possible to match ion currents and concentrations simultaneously. Thus, the two different matching conditions characterise two mutually exclusive network flow models. Hereinafter, we shall use the terms 'matched current model' and 'matched concentration model' to distinguish between the respective solution methods (we continue to use 'network models' to refer to these collectively). For a contraction-expansion having the geometry described previously, both models will give identical predictions for the inlet and outlet sections, but different predictions (in general) for the contraction. We compare these model results with the results of the CFD simulations to examine the validity of the two matching conditions.

C.F.D. METHOD

The electrokinetic flow equations are solved numerically using an adapted single phase version of the transient two-fluid finite volume CFD method due to Rudman (1998). Details of the method as applied to electrokinetic flow are given by Davidson and Harvie (2007). Due to the axial symmetry of the flow, calculations are performed on one symmetric half of the domain ($\hat{y} \geq 0$). A uniform staggered grid with $\delta x = \delta y = 1/32$ is utilised. Grid refinement test calculations in which δx and δy were simultaneously halved led to only minor differences in the

values of the key variables. The potential gradient at the inlet is determined iteratively to give a pressure gradient of approximately zero within the inlet segment. The resulting potential gradients are $\partial \hat{U} / \partial \hat{x} \approx 8.28$ when $K = 2$ and $\partial \hat{U} / \partial \hat{x} \approx 9.50$ when $K = 4$. These values are slightly different to those predicted using the network models owing to the finite resolution of the CFD method. The calculations are taken to be converged to a steady state when the value of each variable is effectively unchanging.

RESULTS AND DISCUSSION

Results are presented for a 1:1 electrolyte solution with $Sc = 1000$ and $B = 2.34 \times 10^{-4}$ (based on the properties of water at a temperature of 298 K) and $Re = 0.01$ (typical of laminar flows encountered in microchannels). We consider two dimensionless inverse Debye lengths, $K = 2$ and $K = 4$, with dimensionless surface charge density $S = 16$. The EDLs are overlapping when $K = 2$.

The results of the finite volume simulations are compared against the predictions of both network models. For the matched current model, the concentration ratios calculated for the contraction are $N_{ci} \approx 1.26$ for $K = 2$ and $N_{ci} \approx 0.72$ for $K = 4$ (as explained above, $N_{kj} = 1$ in all cases when a matched concentration condition is used). Irrespective of the matching condition that is chosen, the model results are expected to differ from the CFD results to some extent. The network models neglect the effects of the converging/diverging flow fields at the entrance/exit of the contraction, and also neglect the influence of the rear/forward facing walls there on the electrostatics. Furthermore, diffusive fluxes due to axial concentration gradients are not accounted for. Nonetheless, any discrepancies are expected to be small within those regions in which the simulated flow is fully developed.

Fig. 2 compares the numerical predictions of the dimensionless cation and anion concentrations at the channel centre-line to the corresponding values calculated using the network models. The CFD results (continuous curves in Fig. 2) for both values of K indicate that at any location along the channel, the cation concentration is lower than the anion concentration. Thus, the fluid bears a net negative charge, which is consistent with the requirement of electroneutrality for the entire solid-fluid system (the channel walls are positively charged). The cation concentration decreases within the contraction because of the positive wall charge and the narrower wall spacing there. The opposite effect occurs for the anions. With regard to the network model results (dashed/dotted lines in Fig. 2), it is clear that the choice of matching condition has a significant impact upon the predicted cation concentrations. The matched current model demonstrates excellent agreement with the fully developed CFD values throughout the domain. However, the matched concentration model produces significant errors within the contraction. For instance, the predicted cation concentration is almost double the simulated value for $K = 4$ when the matched concentration condition is applied. Conversely, the choice of matching condition has little impact on the anion concentrations, although it is again clear that the matched current model yields satisfactory predictions.

Fig. 3a illustrates the dimensionless pressure variation at the centre-line of the channel, and the corresponding pressure gradients (derivatives of the curves in Fig. 3a with respect to the axial coordinate) are shown in Fig. 3b. As a consequence of the imposed electric field, the pressure difference across the entire domain is essentially equal to the pressure drop required to drive flow through the contracted segment alone. It is clear that the gradients determined by CFD are similar to those predicted by both network models when the flow is fully developed.

Sisavath *et al.* (2002) have shown that the overall pressure difference in non-electroviscous creeping flow through a contraction-expansion can be reasonably well approximated by summing the contributions due to fully developed flow in each segment of the channel plus an
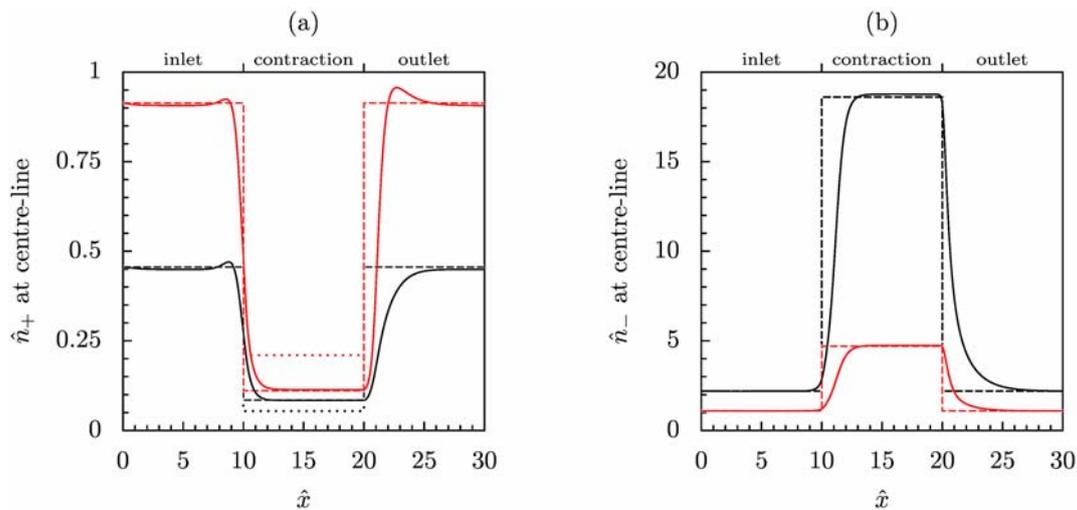
Figure 2: Comparison of predicted concentrations of (a) cations and (b) anions at the channel centre-line ($\hat{y} = 0$) for $K = 2$ (black curves) and $K = 4$ (red curves). Results of the CFD simulations are shown as continuous curves. Appropriately re-scaled solutions derived using the matched current model (dashed lines) and matched concentration model (dotted lines) are also shown. Note that the different matching methods give identical predictions for the inlet and outlet regions, and almost coincident predictions for the anion concentration in the contraction.
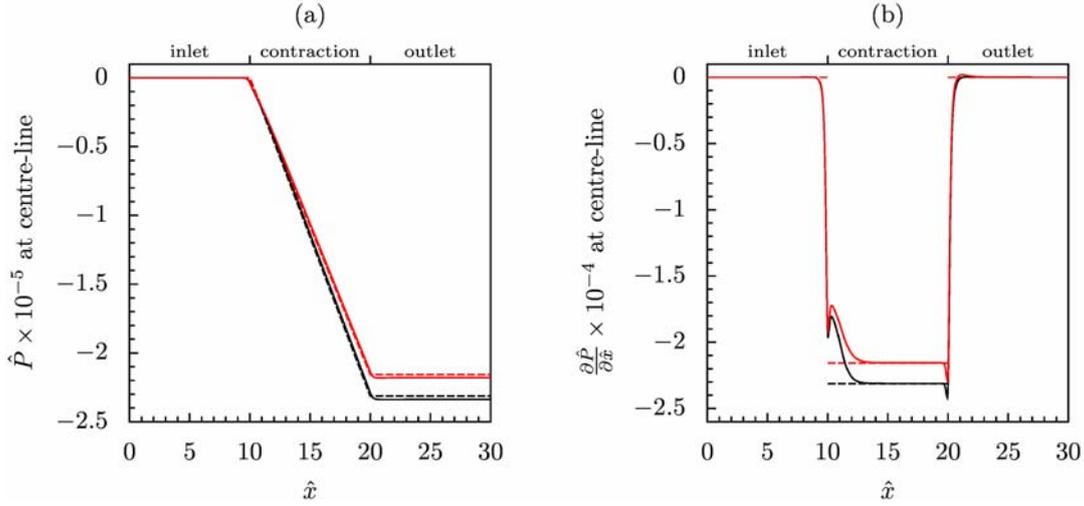
Figure 3: Comparison of predicted (a) pressures and (b) pressure gradients at the channel centre-line. Curve colours and line styles are as in Fig. 2. Note that the matched concentration results are similar to the matched current results and have been omitted for clarity.
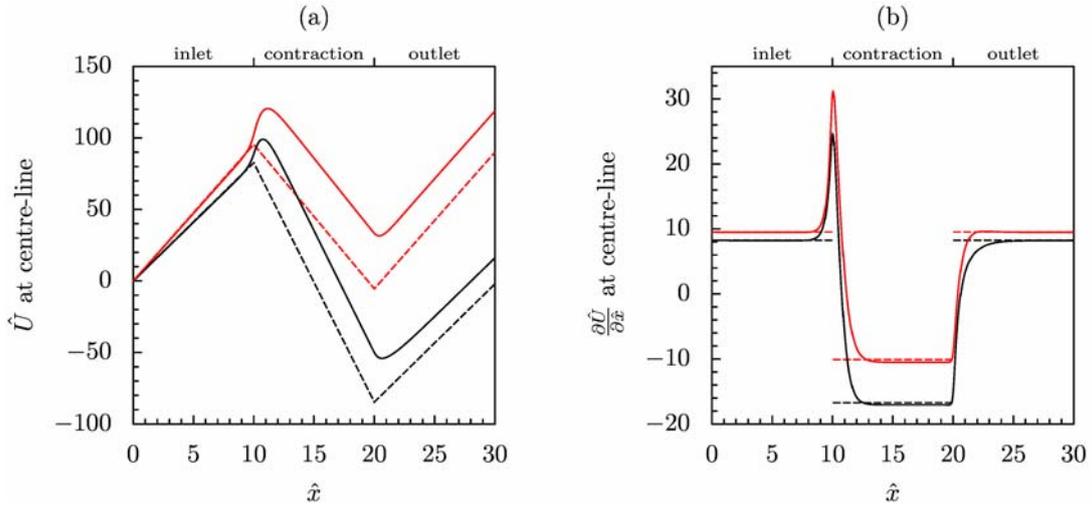
Figure 4: Comparison of predicted (a) potentials and (b) potential gradients at the channel centre-line. Curve colours and line styles are as in Fig. 2. Note that the matched concentration results are similar to the matched current results and have been omitted for clarity.

additional (or excess) pressure difference ΔP_e due to the contraction-expansion:

$$\Delta P_t = \left(\Delta P_i + \Delta P_c + \Delta P_o\right) + \Delta P_e. \qquad (19)$$

Following the same approach and using the matched current model to calculate the fully developed pressure drops for each section of the channel, we find that the excess pressure difference accounts for approximately 1% of the total pressure difference for both cases considered herein. Thus, for these particular sets of physical parameters, the matched current model provides a very good approximation of the true pressure changes occurring over the device.

Fig. 4a shows the variation of the dimensionless total electrical potential at the channel centre-line, and the corresponding potential gradients are shown in Fig. 4b. The potential rises in the inlet and outlet sections of the channel as a result of the imposed electric field. Since this field is such that the pressure gradient is (approximately)

zero in the inlet and outlet regions, the fluid flows solely under the influence of the potential gradient there. The potential rises sharply near the entrance of the contraction, which can be understood in terms of the opposing effects of conduction and diffusion. Cations in the inlet region will tend to diffuse into the contraction where their concentration is lower (Fig. 2a), while the opposite is true for anions, which will tend to diffuse out of the contraction (Fig. 2b). The abrupt rise in potential at the entrance of the contraction applies an electrostatic force on both ions that counteracts these diffusive processes, thus maintaining steady-state concentrations within the channel.

Analogous to the excess pressure difference described above, one may define an excess potential difference:

$$\Delta U_t = \left(\Delta U_i + \Delta U_c + \Delta U_o\right) + \Delta U_e. \qquad (20)$$

In contrast to the pressure results, however, it is apparent that the excess potential difference is quite large,

predominantly due to the diffusive effects addressed above. For instance, for the case of $K = 2$, the overall potential differences predicted by the network models and the CFD simulation have different signs. As such, the models do not give an accurate account of the true potential changes occurring over the device for the cases considered herein. Nevertheless, both models do provide excellent predictions of the potential gradients in regions where the flow is fully developed.

CONCLUSION

Electro-osmotic effects in steady-state flow through a 4:1:4 slit-like microfluidic contraction-expansion at low Reynolds number are investigated using CFD and two network models. The first network model is based on an ion current-matching condition proposed by two of the authors; the second employs a concentration-matching condition found in the literature. We find that the choice of matching condition can have a significant impact on the modelled cation concentrations in the contraction: the matched current model exhibits excellent agreement with the CFD predictions, while the matched concentration model displays sizeable errors. The two models give essentially comparable predictions for the other variables considered.

The matched current model provides an approximate account of the pressure and potential changes that occur over the flow domain. Differences between the model and the true flow conditions (as determined using CFD) can be quantified in terms of excess pressure and potential differences. Correlations for the prediction of these quantities would be of significant benefit to the application of the model as a design tool for microfluidic systems. However, appropriate correlations have yet to be reported in the literature. Work is ongoing to extend the results presented herein to a wider parameter range, which it is hoped will facilitate the development of such relationships in the future.

REFERENCES

AJDARI, A., (2004), "Steady flows in networks of microfluidic channels: building on the analogy with electrical circuits", *C. R. Phys.,* **5,** 539–546.

BAYRAKTAR, T. and PIDUGU, S.B., (2006), "Characterization of liquid flows in microfluidic systems", *Int. J. Heat Mass Transfer,* **49,** 815–824.

BERLI, C.L.A., (2007), "Theoretical modelling of electrokinetic flow in microchannel networks", *Colloids Surf. A,* **301,** 271–280.

BURGREEN, D. and NAKACHE, F.R., (1964), "Electrokinetic flow in ultrafine capillary slits", *J. Phys. Chem.,* **68 (5),** 1084–1091.

DAVIDSON, M.R. and HARVIE, D.J.E., (2007), "Electroviscous effects in low Reynolds number liquid flow through a slit-like microfluidic contraction", *Chem. Eng. Sci.,* **62,** 4229–4240.

DUTTA, P., BESKOK, A., and WARBURTON, T.C., (2002a), "Electroosmotic flow control in complex microgeometries", *J. Microelectromech. Syst.,* **11 (1),** 36–44.

DUTTA, P., BESKOK, A., and WARBURTON, T.C., (2002b), "Numerical simulation of mixed electroosmotic/pressure driven microflows", *Numer. Heat Transfer A,* **41,** 131–148.

GHOSAL, S., (2002), "Lubrication theory for electro-osmotic flow in a microfluidic channel of slowly varying cross-section and wall charge", *J. Fluid Mech.,* **459,** 103–128.

HANSEN, C.L., SKORDALAKES, E., BERGER, J.M., and QUAKE, S.R., (2002), "A robust and scalable microfluidic metering method that allows protein crystal growth by free interface diffusion", *Proc. Natl. Acad. Sci. U.S.A.,* **99 (26),** 16531–16536.

HARVIE, D.J.E. and DAVIDSON, M.R., (2009), "Microfluidic circuit analysis—flowrate and ion current relationships for thin slits and pipes", submitted to *J. Colloid Interface Sci.*

HO, C.-M. and TAI, Y.-C., (1998), "Micro-electro-mechanical-systems (MEMS) and fluid flows", *Annu. Rev. Fluid Mech.,* **30,** 579–612.

HUNTER, R.J., (1981), *Zeta Potential in Colloid Science: Principles and Application,* Academic Press, New York.

LAGALLY, E.T., SIMPSON, P.C., and MATHIES, R.A., (2000), "Monolithic integrated microfluidic DNA amplification and capillary electrophoresis analysis system", *Sens. Actuators B,* **63,** 138–146.

PARK, S.Y., RUSSO, C.J., BRANTON, D., and STONE, H.A., (2006), "Eddies in a bottleneck: an arbitrary Debye length theory for capillary electroosmosis", *J. Colloid Interface Sci.,* **297,** 832–839.

PRAKASH, S., PIRUSKA, A., GATIMU, E.N., BOHN, P.W., SWEEDLER, J.V., and SHANNON, M.A., (2008), "Nanofluidics: systems and applications", *IEEE Sens. J.,* **8 (5),** 441–450.

RUDMAN, M., (1998), "A volume-tracking method for incompressible multifluid flows with large density variations", *Int. J. Numer. Methods Fluids,* **28 (2),** 357−378.

SAUTER, C., DHOUIB, K., and LORBER, B., (2007), "From macrofluidics to microfluidics for the crystallization of biological macromolecules", *Cryst. Growth Des.,* **7 (11),** 2247–2250.

SISAVATH, S., JING, X., PAIN, C.C., and ZIMMERMAN, R.W., (2002), "Creeping flow through an axisymmetric sudden contraction or expansion", *J. Fluids Eng.,* **124,** 273–278.

STONE, H.A. and KIM, S., (2001), "Microfluidics: basic issues, applications, and challenges", *AIChE J.,* **47 (6),** 1250–1254.

UGAZ, V.M., ELMS, R.D., LO, R.C., SHAIKH, F.A., and BURNS, M.A., (2004), "Microfabricated electrophoresis systems for DNA sequencing and genotyping applications: current technology and future directions", *Phil. Trans. R. Soc. Lond. A,* **362,** 1105–1129.

XUAN, X. and LI, D., (2004), "Analysis of electrokinetic flow in microfluidic networks", *J. Micromech. Microeng.,* **14,** 290–298.